EJN fens EUROPEAN JOURNAL OF NEUROSCIENCE

European Journal of Neuroscience, pp. 1–9, 2011 doi:10.1111/j.1460-9568.2011.07627.x

Modulation of dendritic synaptic processing in the lateral superior olive by hyperpolarization-activated currents

Katarina E. Leão,[1,2,*] Richardson N. Leão[2,3,*] and Bruce Walmsley[1]
[1]Synapse and Hearing Laboratory, The John Curtin School of Medical Research, The Australian National University, Canberra, ACT, Australia
[2]Department of Neuroscience, Uppsala University, Biomedical Center, Box 593, Husargatan 3, 751 23 Uppsala, Sweden
[3]Brain Institute, Federal University of Rio Grande do Norte, Natal-RN, Brazil

Keywords: hyperpolarization-activated cyclic-nucleotide-gated type 1 channels, hyperpolarization-activated current, lateral superior olive, superior olivary complex, synchronous excitatory post-synaptic potential

Abstract

We have previously shown that mice lateral superior olive (LSO) neurons exhibit a large hyperpolarization-activated current (I_h), and that hyperpolarization-activated cyclic-nucleotide-gated type 1 channels are present in both the soma and dendrites of these cells. Here we show that the dendritic I_h in LSO neurons modulates the integration of multiple synaptic inputs. We tested the LSO neuron's ability to integrate synaptic inputs by evoking excitatory post-synaptic potentials (EPSPs) in conjunction with brief depolarizing current pulses (to simulate a second excitatory input) at different time delays. We compared LSO neurons with the native I_h present in both the soma and dendrites (control) with LSO neurons without I_h (blocked with ZD7288) and with LSO neurons with I_h only present peri-somatically (ZD7288+ computer-simulated I_h using a dynamic clamp). LSO neurons without I_h had a wider time window for firing in response to inputs with short time separations. Simulated somatic I_h (dynamic clamp) could not reverse this effect. Blocking I_h also increased the summation of EPSPs elicited at both proximal and distal dendritic regions, and dramatically altered the integration of EPSPs and inhibitory post-synaptic potentials. The addition of simulated peri-somatic I_h could not abolish a ZD7288-induced increase of responsiveness to widely separated excitatory inputs. Using a compartmental LSO model, we show that dendritic I_h can reduce EPSP integration by locally decreasing the input resistance. Our results suggest a significant role for dendritic I_h in LSO neurons, where the activation/deactivation of I_h can alter the LSO response to synaptic inputs.

Introduction

Principal neurons of the lateral superior olive (LSO) are located in the brainstem auditory pathways that process signals underlying sound localization. LSO cells are bipolar/multipolar cells that receive excitatory inputs (encoding ipsilateral acoustic information) onto their dendrites and inhibition (encoding contralateral acoustic information) onto their somas (Yin, 2002). Classically, LSO neurons are thought to compute interaural intensity differences by subtracting contralateral inhibition from ipsilateral excitation. However, there is increasing evidence that LSO neurons can also perform more complex computations such as coincidence detection of excitation and inhibition, and phase-lock to amplitude envelopes of high-frequency sounds (Batra *et al.*, 1997; Tollin & Yin, 2005). Furthermore, the dendrites and soma regions of LSO neurons do not behave as passive compartments as would be expected from simple excitatory post-synaptic potential (EPSP)/inhibitory post-synaptic potential integrators, but instead display a variety of voltage-dependent currents that generate non-linear current/voltage relations (Adam *et al.*, 2001). In addition, patch-clamp recordings show that multiple-firing LSO neurons can switch from chopper- to onset-type neurons if hyperpolarizing or depolarizing steps precede test stimulation (Adam *et al.*, 2001).

The LSO dendrites express a variety of ion channels that determine the firing properties of the cell in response to synaptic inputs (Barnes-Davies *et al.*, 2004; Leao *et al.*, 2006). For example, hyperpolarization-activated cyclic-nucleotide gated (HCN) type-1 channels are strongly expressed on LSO neuron dendrites and soma (Leao *et al.*, 2006). HCN1 channels generate a relatively fast type of hyperpolarization-activated current (I_h) and LSO neurons display the fastest and largest I_h in the initial sound localization pathway, comprising the anteroventral cochlear nucleus (AVCN) and the medial nucleus of the trapezoid body (MNTB) (Leao *et al.*, 2006). The LSO I_h modulates resting potential, input resistance and post-inhibition rebound activity (Leao *et al.*, 2006; Szalisznyo, 2006), but the specific function of I_h in the dendrites of LSO neurons is unknown.

Variations of ion channel distribution in different neuronal compartments are important for action potential (AP) generation and synaptic integration. The subcellular localization of I_h in particular has been the subject of intense investigation (Magee, 1999; Berger *et al.*, 2003; Desjardins *et al.*, 2003; Migliore *et al.*, 2004; Nolan *et al.*,

Correspondence: Katarina E. Leão, [2]Department of Neuroscience, as above.
E-mail: Katarina.Leao@neuro.uu.se

*K.E.L. and R.N.L. contributed equally to this work.

Received 4 March 2010, revised 21 December 2010, accepted 10 January 2011

2004; Oviedo & Reyes, 2005). Dendritic I_h is responsible, for example, for normalizing EPSP integration along dendritic branches, causing distal and proximal synaptic inputs to have similar integrative properties (Magee, 1999). In this study, we investigate the effect of I_h in LSO dendrites on the temporal processing of EPSPs. Dendritic I_h was found to modulate the computation of synchronous EPSPs by decreasing temporal summation, and deactivation of I_h (e.g. after spike trains) increased firing in response to asynchronous EPSPs.

Materials and methods

Electrophysiology

Normal mouse (CBA and C57B6) and HCN1-knock-out (KO) mouse (B6;129-Hcn1^{tm2Kndl}/J from Jackson Labs, originally donated by Eric Kandel, Columbia University, New York) brain slices containing the LSO were obtained as described previously (Leao et al., 2006). C57B6 mice were used as a control for experiments involving HCN1-KO mice but the remaining experiments were performed in CBA mice as C57B6 mice undergo age-related hearing loss/deafness in later developmental stages (several months old) (Willott & Erway, 1998). In brief, 17-21-day-old mice (average 19 ± 1 days) were decapitated (for electrophysiology) without anaesthetic according to the Australian National University Animal Ethics Committee protocol. The forebrain and cerebellum were removed and placed in ice-cold sucrose-based solution (Leao et al., 2006). Transverse slices (200 μm) were made of the LSO using an oscillating tissue slicer. Slices were incubated for 1 h in normal artificial cerebrospinal fluid at 35 °C and subsequently held at room temperature (22–25 °C) for electrophysiological recordings using glass pipettes filled with a K^+-gluconate internal solution [containing (in mM): 17.5 KCl, 122.5 K-gluconate, 9 NaCl, 1 $MgCl_2$, 3 Mg-ATP, 0.3 guanosine triphosphate-Tris, 1 HEPES and 0.2 EGTA]. The pipettes had resistances ranging from 2 to 4 MΩ. Only recordings with < 6 MΩ series resistance and > 45 MΩ input resistance were accepted and the capacitance was compensated and bridge balance adjusted using the built-in amplifier circuits. I_h was blocked by the addition of 20 μM ZD7288 (Tocris, UK) or 1 mM CsCl. In all experiments, current was injected to keep the membrane potential at the same voltage prior to I_h block. Data were acquired using a patch-clamp amplifier (Multiclamp 700B, Molecular Devices, USA), low-pass filtered at 10 kHz, digitized at 20 kHz samples/s using Axograph X (Australia) and analysed using Matlab (Mathworks, USA). Neurobiotin (0.5%) or Alexa 488 (Invitrogen) was added to the internal solution in order to determine the spatial position of cells. We restricted our recordings to lateral LSO cells as there is a difference in low-threshold potassium currents between the medial and lateral LSO cells that would obscure the interpretation of the results. EPSPs were evoked in LSO cells by placing a bipolar electrode on the fibre bundle projecting from the ipsilateral AVCN. Data are presented as either mean ± SEM or % of the total population (n). A paired t-test was used to compare differences between means and a Z-test to compare differences between two proportions. Differences were considered significant for $P < 0.05$. Statistical tests were performed in the Matlab + statistics toolbox (Mathworks) or R (http://cran.r-project.org/).

Dynamic clamp

We simulated I_h in LSO neurons using a dynamic clamp. In order to assess the effect of I_h kinetics on cell function, we used a fast I_h based on our previous LSO recordings (Leao *et al.*, 2006). Our dynamic-clamp method was implemented on a second computer running real-time Linux and custom-made software that reads voltage and generates currents at 40 kHz injected by the recording electrode (located at the cell soma). A description of the dynamic-clamp technique can be found in our previous study (Leao *et al.*, 2005). In order to add a macroscopic I_h confined to the cell soma (and perisomatic compartments), we first blocked the 'real' I_h with 20 μM ZD7288 (Tocris). Simulated I_h was calculated by $I_h = \bar{g}_h u(V - V_{rev})$ where $\bar{g}_h$ is the maximal hyperpolarization-activated conductance (between 15 and 30 nS), u is the evolution variable, V is the membrane voltage and V_{rev} is the I_h reversal potential (Leao *et al.*, 2006). Evolution variables were obtained by the following equation

$$\frac{dx}{dt} = \frac{x_\infty - x}{\tau_x}, \quad x = u \tag{1}$$

The activation time constant vs. voltage [$\tau_x(V)$] and steady-state conductance vs. voltage (Boltzmann) functions for I_h were, respectively

$$\tau_u(V) = \frac{10000}{234.5878e^{0.0648(V+20.049)} + 5.28e^{-0.0369(V+20.049)}} + 7.08 \tag{2}$$

$$u_\infty(V) = \left(1 + e^{0.144(V+82.6)}\right)^{-1} \tag{3}$$

These equations were obtained by fitting the time constants of I_h and the normalized I_h conductance across various voltages from I_h recordings of LSO cells shown in our previous work (Leao *et al.*, 2006). Note that the Boltzmann relations shown here refer to steady-state conductance, not steady-state current. The amplitude of the simulated current was adjusted to match the 'real' I_h from the recorded cell.

Immunohistochemistry

Slices were obtained as described above and fixed for 1 h in 4% paraformaldehyde in phosphate-buffered saline (17.52 g NaCl, 0.4 g KCl, 100 mL of 0.2 M phosphate buffer, 1.9 L distilled water). Free-floating slices were blocked in antibody solution (5% normal donkey serum in phosphate-buffered saline with 0.3% Triton-X-100) for 30 min. Primary antibodies against HCN1, HCN2 and HCN4 (1 : 500) were purchased from Alomone (Israel) (catalogue nos APC-056, APC-030 and APC-052, respectively) and microtubule-associated protein 2A/B (MAP2A/B) (1 : 200, MAB3418, Millipore, USA) was used to label somas and dendrites. Slices were incubated in primary antibodies overnight with constant agitation at room temperature. After washing the sections three times in phosphate-buffered saline for 20 min, slices were incubated with species-appropriate Alexa-conjugated secondary antibodies (1 : 1000, Invitrogen) for 1 h with agitation. Sections were then washed as above in phosphate-buffered saline and mounted on glass slides with Vectashield mounting media (Vector Labs) and kept in the dark until examined on a confocal laser scanning microscope (Carl Zeiss). Antigen colocalization was calculated according to Leão *et al.* (2010).

Lateral superior olive model

We constructed a simplified LSO model consisting of 10 dendritic compartments and a soma. The soma compartment contained a fast inactivating Na^+ current (I_{Na}), a low-threshold (I_{Kl}) and high-threshold (I_{Kh}) voltage-dependent K^+ current, I_h and a non-specific leakage current (I_l). Dendritic compartments were supplied with I_h and a non-specific leakage current (I_l).

I_{Na}, I_{Kl} and I_{Kh} equations are described in Rothman & Manis (2003) and passive parameters are found in Zacksenhouse *et al.* (1998). Each dendritic compartment was simulated by a cylinder of 3 μm diameter and 20 μm length and the soma was a sphere of 20 μm diameter. The total Na^+, low- and high-threshold K^+ conductances were equal to 200, 15 and 20 nS, respectively. The maximal I_h conductance was equal to 4 mS/cm^2 in all compartments unless otherwise stated. In one set of simulations, we modelled 10 excitatory synapses on the dendrite. Synaptic conductances were modelled by alpha functions ($x_{e,j} = t_{e,j}\exp[(1 - t_{e,j})/\tau_p]$, per τ_p) with a time constant τ_p (0.15 ms) and $t_{e,j}$ as the time of the last synaptic event at the terminal j. Synaptic currents I_{syn} (I_e) were modelled by $I_e = g_e x_e(V - V_e)$ where V_e is the reversal potential for excitatory (0 mV) synapses and g_e is the total synaptic conductance (0.005 nS).

Results

We recorded from 40 LSO cells from normal (CBA) mice, four cells from normal (C57B6) mice and eight cells from HCN1-KO mice. We targeted principal cells localized in the lateral limb of the LSO. There were no significant differences between CBA and C57B6 mice at the age range used for any of the results reported in this work. In order to identify LSO principal neurons (due to the presence of lateral olivary complex neurons within the LSO perimeter), we verified the presence of a large I_h (inward currents > 2 nA at −100 mV) in normal mice or the time-course of evoked EPSPs in HCN1-KO mice. In both normal (CBA and C57B6) and HCN1-KO mice we found a predominance of single-firing LSO cells in the lateral region of the nucleus consistent with Barnes-Davies *et al.* (2004).

Membrane properties were significantly changed by the blockage of I_h with 20 μM ZD7288, which increased the input resistance from 67.3 ± 5.4 to 103.5 ± 6.2 MΩ ($P = 0.002$, $n = 24$, paired t-test). The addition of an artificial I_h using dynamic clamp decreased the mean input resistance (after ZD7288 application) to 69.5 ± 7.3 MΩ (not significantly different from control conditions; $n = 24$). Similar to our previous work, the resting membrane potential was equal to −57.8 ± 0.7 mV before and −65.2 ± 3.7 mV after ZD7288 addition ($P = 0.001$, $n = 24$, paired t-test). The application of single shocks elicited EPSPs with a mean half-width of 3.3 ± 0.1, 5.7 ± 0.4 and 3.5 ± 0.1 ms in control conditions, in the presence of 20 μM ZD7288 and in the presence of dynamic clamp, respectively ($P = 0.0002$, $n = 24$, ANOVA). When control and ZD7288 conditions were compared using paired t-test, $P = 0.0004$ ($n = 24$) and $P = 0.01$ when control and dynamic clamp were compared ($n = 24$).

Simulated peri-somatic hyperpolarization-activated currents does not efficiently prevent synaptic summation

To study the synaptic summation of excitatory inputs we applied 10 pulses at 50 Hz to elicit EPSPs using a bipolar electrode. The temporal summation was estimated using the area underneath the curve of EPSPs vs. time (EPSP integral) divided by the amplitude of the first EPSP in the train (temporal summation index) (Fig. 1A). In CBA mice, mean amplitudes for the first EPSP in the train were equal to 4.2 ± 0.5, 6.0 ± 0.5, 5.6 ± 0.4 and 4.5 ± 0.5 mV for control, 20 μM of ZD7288, 20 μM of ZD7288+ injected current (bringing the potential back to resting values before ZD7288 application) and dynamic clamp, respectively (Fig. 1B). The first EPSP amplitudes were significantly different between control and ZD7288 ($P = 0$, $n = 24$, paired t-test), and between control and dynamic clamp ($P = 0$, $n = 24$, paired t-test; Fig. 1C). Current injection (ZD7288+ injected current) also significantly decreased the first EPSP amplitude when compared with ZD7288 alone ($P = 0.011$, $n = 24$, paired t-test). The average temporal summation index for control, ZD7288, ZD7288+ injected current and dynamic clamp in CBA mice was equal to 3.1 ± 0.3, 9.2 ± 1.3, 12.2 ± 1.7 and 5.0 ± 0.6 ms, respectively (Fig. 1C). Paired t-tests between control vs. all other conditions and dynamic clamp vs. all other conditions showed P values <0.01 but no significant difference was found between the mean EPSP integrals without and with current injection when ZD7288 was present in the bath.

Native, but not simulated, hyperpolarization-activated current decreases the time window for firing in response to multiple excitatory inputs

Using a brief (1 ms) current pulse applied to the patch pipette concomitantly to evoke simulated EPSPs, we analysed the LSO cell's

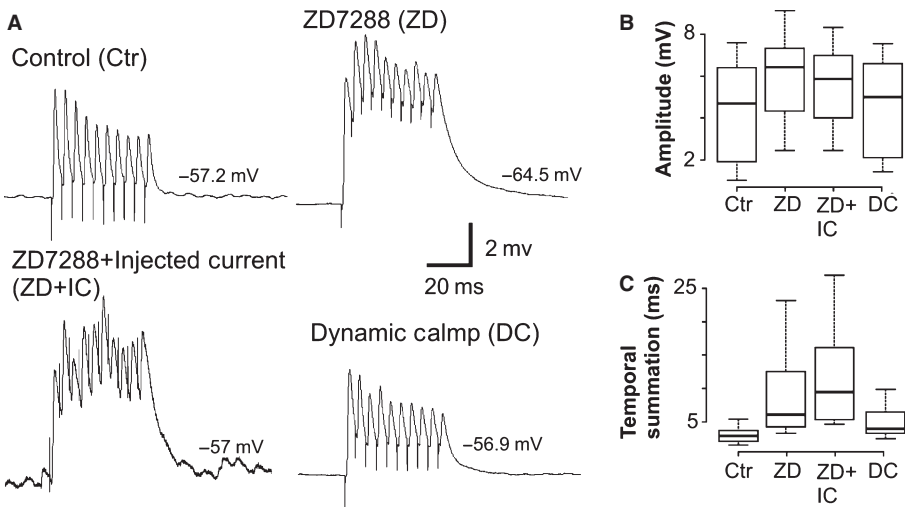

FIG. 1. I_h is essential for minimizing temporal summation in normal mice. (A) Membrane voltage changes in response to a train of evoked EPSPs in control (Ctr) conditions (upper left), after application of ZD7288 (ZD) (upper right), ZD and an injected depolarizing current [ZD+ injected current (IC), lower right] and after the addition of an artificial I_h in the presence of ZD using dynamic clamp (DC, lower left). Resting membrane potentials for each condition are shown on the right. (B) Average amplitude of the first EPSP in the train. (C) Summary of temporal summation index (area under the curve divided by the amplitude of the first EPSP in the train).

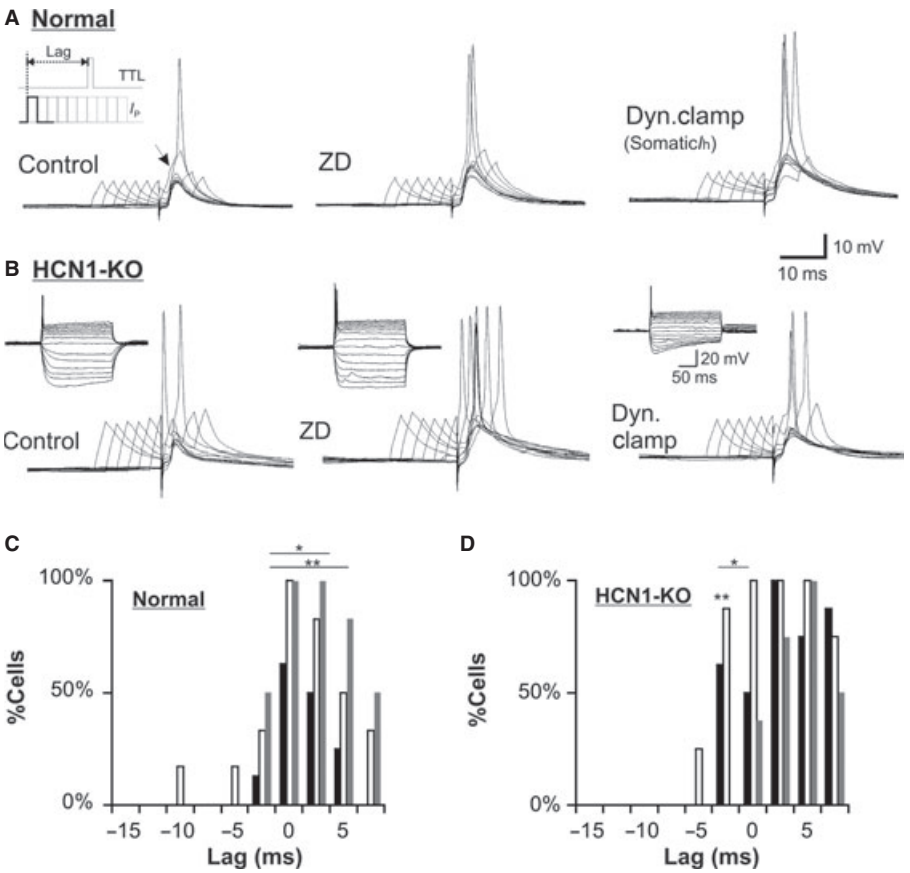

FIG. 2. I_h improves the detection of synchronous excitatory inputs. Representative example of the response of LSO neurons from a normal (CBA) (A) and an HCN1-KO (B) mouse to the application of a current pulse and a lagged electrical stimulus (to evoke a subthreshold EPSP, see text, left inset). The panels show the voltage responses to the coincidence detection protocol in normal mice (CBA) in control conditions (left), in the presence of ZD7288 (ZD) in the bath (middle) and in the presence of ZD and a simulated I_h [dynamic clamp (Dyn. Clamp), right]. Insets in B show current-clamp recordings of a neuron from an HCN1-KO mouse in response to current steps ranging from −350 to +300 pA. Percentage of cells that fired APs in response to the current pulse/EPSP stimulation at different lags in control conditions (black bars), in the presence of ZD7288 (white bars) and in ZD plus the artificial I_h (Dyn. Clamp, grey bars) in normal (CBA) (C) and HCN1-KO (D) mice. *$P < 0.05$; **$P < 0.01$; TTL, Transistor-Transistor Logic.

ability to fire to time-separated excitation. We kept the time of the EPSP trigger [Transistor-Transistor Logic (TTL)] pulse fixed and varied the onset of the current pulse around the EPSP trigger pulse time in 2.5 ms steps (Fig. 2A). The amplitude of the current step was set according to the cell's firing threshold by increasing the pulse amplitude by 50 pA until producing an AP and then subtracting 50 pA. The initial EPSP/current step lag was '−15 ms' (current step applied 15 ms before the trigger pulse to the stimulator; Fig. 2A). Note that the 'lag' is in relation to the time difference between the current pulse (from the patch amplifier) and the time of a trigger pulse (from the bipolar electrode). The evoked EPSP time was delayed by an average of 0.9 ± 0.6 ms from the trigger time (Fig. 2A). Figure 2C shows the percentage of cells that fired an AP at a given stimuli lag in control conditions, following ZD7288 application and with peri-somatic I_h simulated by a dynamic clamp. In control conditions, 62.5% (15/24) of cells fired an AP with coincidental stimulus pulse (time of injected current pulse preceding the stimulation shock) and current injection with 0 lag (Fig. 2C). However, in the presence of ZD7288, all cells fired APs when the stimulus pulse and current injection were applied simultaneously (0 lag), independently of the application of the simulated I_h by dynamic clamp ($P = 0.009$, Z-test). In addition, cells fired substantially more APs in response to pulse/current injection for all lags ranging from −2.5 to 5 ms in the presence of ZD7288 (without the dynamic clamp) and −2.5 to 7.5 ms with the dynamic clamp (Fig. 2C). It has been reported that ZD7288 acts on pre-synaptic terminals in a mechanism that is independent of I_h (Chevaleyre & Castillo, 2002). Hence, we have also applied 1 mM CsCl to block I_h in 12 lateral LSO neurons using the same protocol as described above (Supporting Information Fig. S1A and B). The resting membrane potential was equal to −58.4 ± 1.1 mV before and −62.1 ± 4.1 mV after CsCl addition ($P = 0.012$, $n = 12$, paired t-test). In control conditions, two cells (16.7%) fired APs with a stimulus pulse and current injection lagged by 5 ms and no cells fired in response to a 7.5 ms stimuli lag (Supporting Information Fig. S1A and B). However, following the application of 1 mM CsCl, 83.3% (10 cells) of the cells fired APs for stimuli applied with a 5 or a 7.5 ms lag ($P = 0.049$ for both comparisons, Z-test; Supporting Information Fig. S1A and B). We applied the EPSP/current step protocol described above in 12 cells to investigate whether the I_h dependence on temperature would alter our results. At near physiological temperature (35 °C), ZD7288 augmented the number of cells that fired APs when non-synchronous inputs were applied (Supporting Information Fig. S1C and D). At near physiological temperature, 16.7% of cells ($n = 12$) fired APs in response to stimuli lagged by 2.5 ms, whereas 50% of cells ($n = 12$) fired APs in the presence of ZD7288 to the same stimulus ($P = 0.041$, Z-test; Supporting Information Fig. S1C and D).

We have also used the aforementioned protocol to analyse whether HCN1 subunits are necessary to decrease synaptic integration in LSO

dendrites. At 0 ms lag, 50% of the cells of HCN1-KO mice fired APs in control conditions. Application of the I_h blocker ZD7288 caused all cells to fire APs at 0 ms lag ($P = 0.040$, Z-test; Fig. 2B and D) and the addition of the dynamic clamp caused a decrease in the proportion of cells that fired APs to 37.5% ($P = 0.019$ when compared with the ZD7288 condition and not significant when compared with the control condition, $n = 8$; Fig. 2B and D). For lags ≥ 2.5 ms, there was no significant difference in the number of cells that fired APs between all of the experimental conditions (control, ZD7288 and dynamic clamp) in HCN1-KO mice (Fig. 2B and D).

Hyperpolarization-activated cyclic-nucleotide gated type-1-knock-out mice show slower hyperpolarization-activated current

Using immunohistochemistry, we assessed the expression of HCN1 and HCN4 I_h subunits in HCN1-KO mice. It is important to note that C57B6 mice were used as controls in these experiments (see Materials and methods). HCN1-KO mice showed no expression of HCN1 subunits in the LSO, as expected; however, the expression of HCN4 subunits appeared HCN1-like (as in the LSO of CBA and C57B6 mice) with strong expression in cell membranes and dendrites (Fig. 3A and B). In normal animals (CBA and C57B6 mice), HCN1 channels are abundantly labelled in the dendritic and somatic membranes of LSO neurons (Leao *et al.*, 2006; Fig. 3B), whereas HCN4 is moderately expressed in the somas of LSO neurons and HCN2 expression is nearly absent (Leao *et al.*, 2006; Supporting Information Fig. S2). To verify whether HCN1 was located pre- or post-synaptically in normal (CBA) mice, we counted high-intensity pixels (2 SDs greater than the mean pixel intensity) that were and were not colocalized with MAP2A/B. The majority (89.4%) of high-intensity pixels were colocalized with MAP2A/B ($P = 0$, Z-test). In addition, there was no clear medio-lateral gradient of HCN1 expression in the LSO (Leao *et al.*, 2006; Supporting Information Fig. S2). The lack of gradient is also supported by electrophysiological data (Barnes-Davies *et al.*, 2004; Leao *et al.*, 2006). When compared with normal mice, the I_h amplitude in LSO neurons of HCN1-KO mice is drastically smaller and the current activation is significantly slower (at −100 mV, total inward currents were equal to −0.37 ± 0.06 nA with an activation time constant equal to 515 ± 53 ms, compared with −2.3 ± 0.4 nA and 139 ± 13 ms, respectively, in C57B6 mice; $n = 16$, $P = 0.021$ for both values; Fig. 3C and D). In addition, in LSO neurons of HCN1-KO mice, the temporal summation of EPSPs is not radically affected by the I_h blocker ZD7288 as it is in C57B6 mice (Fig. 3E). The first EPSP amplitudes in HCN1-KO mice showed a small but significant difference between control and ZD7288 (5.2 ± 1.9 vs. 5.7 ± 1.1 mV, respectively, $P = 0.042$, $n = 8$, paired t-test), and between control and dynamic clamp (4.5 ± 0.9 mV, $P = 0.03$, $n = 8$, paired t-test). The EPSP-train summation index in LSO neurons of HCN1-KO mice in

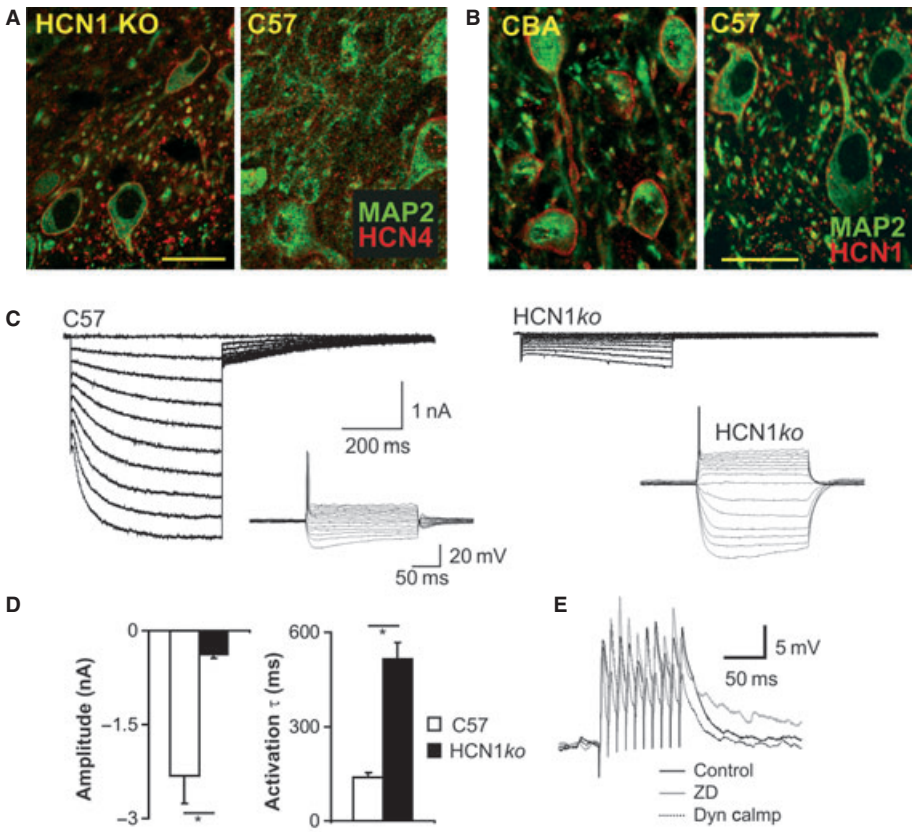

FIG. 3. HCN4 expression is increased in LSO neurons of HCN1-KO mice. (A) HCN4 expression in lateral LSO neurons (labelled with MAP2A/B) in HCN1-KO and C57B6 mice. (B) Examples of HCN1 and MAP2A/B in the lateral third of the LSO from CBA and C57B6 mice. (C) Example of inward currents elicited by voltage steps ranging from −60 to −130 mV recorded from an LSO neuron of a C57B6 mouse (left) and from an HCN1-KO mouse (right). Insets show membrane voltages in response to current injections ranging from −300 to +300 pA from the same cells. (D) Summary of current amplitude and activation time constants of inward currents recorded at −100 mV from C57B6 (white bars) and HCN1-KO (black bars) mice ($n = 16$, $^*P < 0.02$). (E) Membrane voltage changes in response to a train of evoked EPSPs in control conditions, after application of ZD7288 and after the addition of an artificial I_h (in the presence of ZD7288) using dynamic clamp in an LSO neuron of an HCN1-KO mouse.

control conditions was equal to 6.9 ± 1.1 ms (vs. 3.3 ± 0.5 ms in C57B6 mice; $n = 12$, six HCN1-KO cells and six C57B6 cells, $P = 0.012$), and 9.4 ± 1.7 ms in the presence of ZD7288 (vs. 9.1 ± 1.6 ms in C57B6 mice, not significant, $n = 12$) (Fig. 3E). When I_h was applied to LSO cells in HCN1-KO mice using the dynamic clamp, the EPSP-train integral divided by the first EPSP amplitude was equal to 4.8 ± 0.6 ms (vs. 4.3 ± 0.4 ms in C57B6, not significant, $n = 12$).

Native, but not simulated, hyperpolarization-activated current decreases temporal summation of different subthreshold synaptic inputs

In order to assess the role of I_h in the integration of real synaptic inputs, seven LSO neurons were filled with Alexa 488 dye to determine the trajectory of dendrites for positioning the stimulating electrodes. We placed two monopolar stimulating electrodes (glass pipettes filled with artificial cerebrospinal fluid) proximally and distally to the soma (Fig. 4A). We then applied electrical stimuli using two stimulators with various lags (−15 to 7.5 ms in 2.5 ms steps; Fig. 4A and B). To verify if the stimulating electrodes were activating distinct synaptic terminals, we compared the rise times of EPSPs evoked by electrodes 1 (1.1 ± 0.6 ms) and 2 (1.9 ± 0.7 ms, $P = 0.019$, $n = 7$, paired *t*-test) (Fig. 4A). In control conditions, the depolarization amplitude caused by both EPSPs was larger at 0 ms (amplitude equal to 4.9 ± 2.1 mV) stimuli lag when compared with lags of −5 ms (3.6 ± 2.2 mV) or 5 ms (3.2 ± 1.2 mV) ($P = 0.039$ and $P = 0.031$, respectively, $n = 7$, paired *t*-test; Fig. 4A and B). In the presence of 20 μM ZD7288, there was no difference in the depolarization peak amplitudes between different lags (Fig. 4A). In the presence of the dynamic clamp, we observed a significant difference between the depolarization amplitude of stimuli lagging 0 and 5 ms (3.8 ± 1.1 and 2.4 ± 0.7 mV, respectively, $P = 0.012$, $n = 7$; Fig. 4A and B).

Next, we examined the LSO cell's integration of inhibition and excitation with and without I_h. We placed bipolar electrodes on the fibre tract that exits the ipsilateral AVCN to innervate the LSO and in the ipsilateral MNTB (Fig. 4C). The strength of excitation and inhibition was determined by the stimulation frequency rather than amplitude as changing the stimulation amplitude did not produce a smoothly-graded change in excitation or inhibition strength. The stimulation protocol consisted of 40 pulses applied to the MNTB (inhibitory) and 50 pulses applied to the fibre tract arising from the AVCN (excitatory) (Fig. 4D). The excitation pulse frequencies were equal to 62.5, 77.7 and 100 Hz and the respective inhibition pulse frequencies were equal to 50, 66.6 and 100 Hz (excitation : inhibition ratios equal to 1.25, 1.16 and 1; Fig. 4D). When I_h was intact, the normalized number of APs (number of APs in an episode divided by the maximum number of APs fired during the three episodes) was equal to 0.3 ± 0.05, 0.7 ± 0.07 and 1 for excitation : inhibition ratios equal to 1, 1.16 and 1.25, respectively

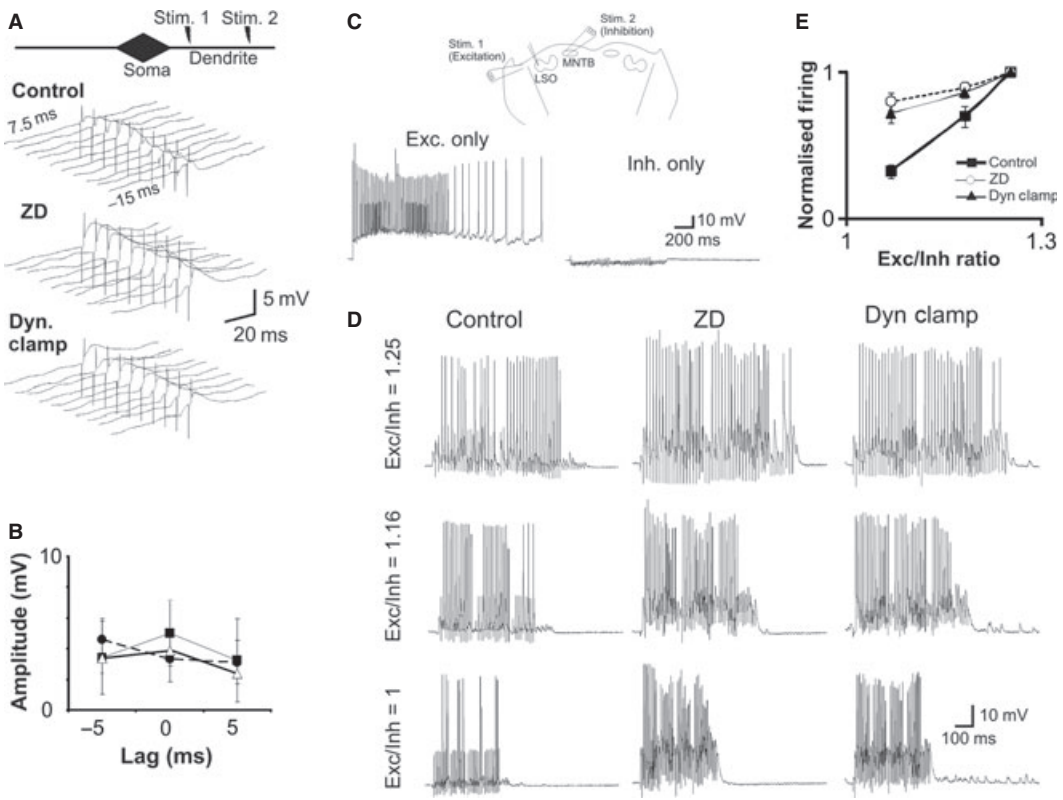

FIG. 4. Native but not dynamic-clamp I_h decreases temporal summation of spatially distinct synaptic inputs. (A) Diagram representing the placement of two stimulating electrodes (Stim. 1 and Stim. 2) in relation to an LSO cell dendrite (top). Bottom panels show an example of recordings of an LSO neuron in response to double synaptic stimulation at various lags between Stim. 1 and Stim. 2 in control, ZD7288 (ZD) and dynamic-clamp (Dyn Clamp) conditions. (B) Summary of compound EPSP amplitude vs. electrical stimuli lags (solid black trace/squares, control; dashed black trace/circles, ZD; solid grey trace/triangles, Dyn Clamp). (C) Diagram showing the placement of bipolar stimulating electrodes to elicit excitation (by stimulating AVCN axons) and inhibition (by stimulation of MNTB neurons) (top) and examples of a neuron response to the stimulation of AVCN axons alone (left trace) or MNTB alone (right trace) (bottom). (D) Membrane potential of a neuron after the stimulation of AVCN axons and MNTB with various frequencies (see text) in control and in the presence of 20 μM ZD and the Dyn Clamp. The ratios between AVCN axon stimulation (excitation) and the MNTB stimulation (inhibition) are shown on the left. (E) Summary of firing ratio vs. excitation : inhibition ratio for control, ZD and Dyn Clamp conditions. Exc., Excitatory; Inh., Inhibitory.

(n = 4; Fig. 4D and E). In the presence of 20 μM ZD7288, these ratios were equal to 0.8 ± 0.06, 0.9 ± 0.02 and 1, respectively (n = 4; Fig. 4D and E) and if the dynamic clamp was applied, these ratios were equal to 0.7 ± 0.07, 0.9 ± 0.03 and 1, respectively (n = 4; Fig. 4D and E). When I_h was intact, there was a stronger correlation between inhibition strength and firing rate. Linear fits for the firing vs. excitation : inhibition ratios relationship produced slopes of 2.6 ± 0.16, 0.77 ± 0.25 and 1.07 ± 0.27 for control, ZD7288 and dynamic-clamp conditions ($P < 0.01$ for all comparisons in relation to control, paired t-test, n = 4).

Dendritic hyperpolarization-activated current decreases local input resistance in lateral superior olive compartmental model

Using a multicompartment LSO cell model we further investigated the role of I_h in dendritic EPSP processing. In Fig. 5A, our model shows that preceding hyperpolarization (applied at the soma, 100 ms before EPSPs were elicited) can provoke a decrease in temporal summation, whereas a leak current is not affected by a pre-test hyperpolarization current step. Figure 5B shows the effect of a preceding hyperpolarizing step (500 ms long) on the input resistance measured at different dendritic compartments in a model with and without dendritic I_h. The input resistance was measured by applying three 10-ms-long current steps (−10, 0 and +10 pA). The graphs in Fig. 5B show the decrease in input resistance in relation to the compartment's resistance without a preceding hyperpolarizing step. The effect of hyperpolarization applied to the soma had a greater effect in decreasing input resistance at peri-somatic compartments (being the 10th compartment closest to the soma) than at distal dendritic compartments. In addition, the lowering of input resistance due to the hyperpolarizing step lasted for about 500 ms, reflecting the slow deactivation of I_h.

Discussion

Previous studies have demonstrated the importance of I_h in modulating cell excitability in auditory neurons (Banks *et al.*, 1993; Bal & Oertel, 2000; Koch & Grothe, 2003; Leao *et al.*, 2005, 2006; Yamada *et al.*, 2005). However, the effects of I_h in the dendrites of auditory neurons have not been systematically investigated. I_h compartmentalization is crucial for its function. For example, Kim *et al.* (2007) have shown that in the calyx of Held, the blockage of I_h hyperpolarizes the terminal by more than 15 mV, whereas in the bushy cell soma, the hyperpolarization is a mere 2.5 mV. In this study a series of electrophysiological techniques, immunohistochemistry and computational modelling were used in order to assess the effect of dendritic I_h on LSO processing. First, using a dynamic-clamp system, we demonstrated that the application of a simulated I_h via a point process to the peri-somatic region does not minimize EPSP summation as intact I_h does. When the dendritic I_h was intact, neurons fired preferentially to synchronous EPSPs. In addition, by stimulating excitatory and inhibitory inputs to the LSO, we demonstrated that blocking the native I_h unbalances the computation of excitatory/inhibitory inputs that, in turn, could reduce the sensitivity of the cell to interaural sound level differences.

Different to MNTB and AVCN neurons, LSO cells show large and fast I_h correlating with strong HCN1 channel expression (Leao *et al.*, 2006). Our immunohistochemistry results suggest that HCN1 channels are present in both LSO cell soma and dendrites. As

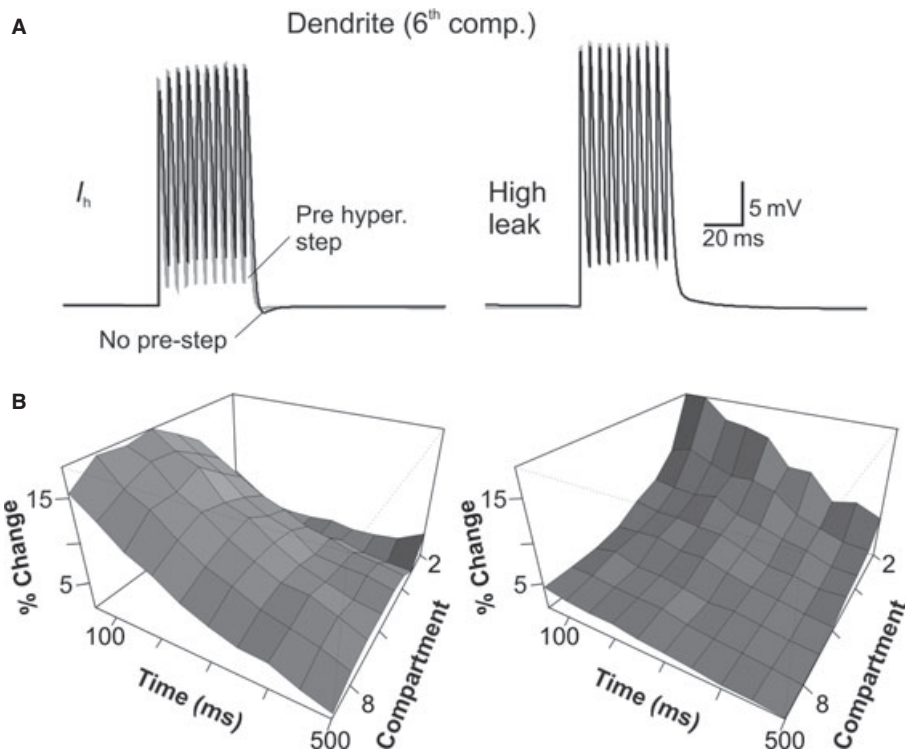

FIG. 5. Dendritic I_h reduces EPSP integration in an LSO cell model. (A) Model response to a train of EPSPs applied at the sixth dendritic compartment. The left panel shows a model in which I_h was present at the dendrite. It shows a decrease in temporal summation when a 500-ms-long, −150 pA hyperpolarizing step was applied prior to the EPSPs (grey trace). If a leak conductance of the same value was present at the dendrite instead of I_h, a pre-hyperpolarization had no effect on EPSPs. (B) Percentage change in input resistance measured locally at different dendritic compartments in relation to the time after the application of a hyperpolarizing step (500 ms long, −150 pA).

AVCN cells also express HCN1 (Leao *et al.*, 2006), the source of HCN1 staining surrounding LSO dendrites could be pre-synaptic terminals. Nevertheless, most of the HCN1 staining found in the LSO is likely to be post-synaptic given the colocalization of HCN1 with MAP2A/B expression, and the large and fast I_h observed in LSO cells.

Using a double-excitation protocol (EPSP and depolarizing pulses) we showed that dendritic I_h prevents the firing in response to asynchronous excitatory inputs. The stimulation of nerve fibres probably elicits EPSPs in LSO cell dendrites, whereas the current injection via the patch pipette affects the soma and peri-somatic compartments. I_h in LSO dendrites will decrease the local input resistance (and consequently the membrane time constant), hence 'sharpening' EPSPs locally, minimizing temporal summation. Although voltage-independent leak channels could produce similar effects, these channels cannot be modulated by membrane potential.

Our dynamic-clamp experiments revealed that, if applied via a point process at the soma, I_h does not shorten the time window for firing in response to coincident inputs but, instead, increases the number of APs in response to our double-excitation protocol. It has been shown that I_h in different neuronal compartments can cause opposite effects on cell firing. For example, dendritic I_h can decrease excitability by reducing temporal summation, whereas somatic I_h increases excitability by depolarizing the resting membrane potential (Santoro & Baram, 2003).

To emulate synaptic currents from proximal and distal dendrites, we used a current-clamp protocol consisting of stimulation of synaptic terminals concomitantly with current injection via somatic patch pipettes. The latter would simulate synaptic currents arising from the proximal dendrite (Ulrich & Stricker, 2000) as excitatory pre-synaptic terminals were found all along LSO principal cell dendrites (Schwartz & Eager, 1999). Confined to peri-somatic compartments (dynamic clamp), I_h caused an increase in cell excitability when compared with conditions in which native I_h was intact. This demonstrates the importance of the subcellular localization of this current and the relationship between localization and function (Santoro *et al.*, 1999). Magee (1998) has shown that dendritic I_h dampens dendritic excitability and our previous work has shown an opposite effect of somatic I_h (increase in cell excitability) (Leao *et al.*, 2005, 2006). In other systems, dendritic I_h decreases temporal summation and normalizes EPSP amplitudes across the dendritic 'cable' (Berger *et al.*, 2003). I_h in LSO neurons also decreases temporal summation of dendritic EPSPs and its effect is modulated by activity history (previous depolarization or hyperpolarization). Previous depolarizations deactivate I_h, increasing temporal summation, whereas hyperpolarization will decrease temporal summation.

This work proposes that dendritic I_h can prevent asynchronous inputs from causing AP firing and this effect is, in turn, controlled by the preceding activity. In other words, dendritic I_h could be activated/deactivated by inhibitory post-synaptic potentials/EPSPs (respectively), changing the processing mode of the dendrite from synchronous input detection to integration. In a previous report, we have shown that the predominant I_h channel type in LSO neurons is HCN1, whereas other HCN subtypes are prevalent in other superior olivary complex nuclei (Leao *et al.*, 2006). HCN1 channels produce the fastest form of I_h with little metabotropic dependency (Pape, 1996). Thus, the preceding neural activity may have a stronger effect on the control of integration of synaptic currents by I_h than second-messenger mechanisms in dendrites that express mostly the HCN1 isoform. Local depolarizations from EPSPs might therefore regionally deactivate I_h (Magee, 1999). Due to slow I_h time constants, the effects of activation/deactivation of I_h can cause relatively long-lasting effects on firing properties of the cells. Also, as demonstrated by our results obtained from HCN1-KO mice, I_h produced by HCN1 channels is more efficient in minimizing temporal integration than other channel subtypes. In addition, an LSO compartmental model supported our experimental results by demonstrating that a relatively fast dendritic I_h is essential to prevent temporal summation of non-coincidental EPSPs. HCN1 channels are not only faster, but they activate at a more positive voltage than other HCN subtypes (Leao *et al.*, 2006). Hence, a greater number of channels would be active at rest, leading to a lowering of input resistance. In addition, the deactivation of I_h could be one of the mechanisms of the switch of firing modes (from tonic to onset firing if inhibition precedes excitation) observed *in vivo* in the LSO (Tsuchitani, 1988).

The detection of synchronous EPSPs may be important for the ability of LSO cells to phase-lock to the amplitude envelope of high-frequency sounds. In other words, LSO neurons would preferably fire when receiving synchronous EPSPs, arriving from AVCN bushy cells of distinct characteristic frequencies (Marsalek & Kofranek, 2005).

The pre-processing of EPSPs by the dendrite is crucial to the integration of these inputs with somatic inhibitory post-synaptic potentials. In fact, a greater EPSP summation in the dendrite associated with a low inhibitory post-synaptic potential summation at the soma could lead to an 'over-representation' of the excitation and, consequently, a lower interaural sound level difference sensitivity. By simultaneously stimulating AVCN fibres and the MNTB, we demonstrated that, when I_h was intact, the firing ratio of LSO neurons was more 'sensitive' to variations on the excitation/inhibition balance and a peri-somatic I_h did not significantly improve the sensitivity to excitation/inhibition variation. In addition, using an LSO cell model, we demonstrated that, when I_h was implemented in the dendrite, the firing ratio vs. excitation : inhibition ratio relation produced a sigmoidal curve similar to *in vivo* interaural sound level difference recordings (Tollin & Yin, 2005) and the model with I_h present only in the soma showed a rapid saturation of firing ratio after excitation surpassed inhibition.

In summary, the present study has investigated the response of LSO neurons to synchronous and asynchronous inputs using simple combinations of stimulated EPSPs and depolarizing current pulses, as a means of gaining insight into the effects of I_h and, in particular, dendritic I_h in LSO neurons. These results demonstrate that 'compartmentalized' I_h can control the firing mode of LSO neurons (synchronicity detectors or integrators) and dendritic I_h plays an essential role in the computation of synaptic inputs in the superior olivary complex.

Supporting Information

Additional supporting information may be found in the online version of this article:

Fig. S1. CsCl and ZD7288 (ZD) show a similar effect on coincidence detection. (A) Voltage responses to the coincidence detection protocol in control conditions and in the presence of 1 mM CsCl in the bath. (B) Percentage of cells that fired APs in response to the current pulse/EPSP stimulation at different lags in control conditions (black bars) and in the presence of CsCl (white bars). (C) Voltage responses to the coincidence detection protocol at 35 °C in control conditions and in the presence of ZD. (D) Percentage of cells that fired APs in response to the current pulse/EPSP stimulation at different lags at 35 °C (black bars, control; white bars, ZD). $*P < 0.05$, *Z*-test.

Fig. S2. HCN1 and HCN4 are expressed across the LSO with no medio-lateral gradient. HCN1 (left) and HCN4 (right) expression across the LSO of two normal mice (CBA). L, lateral.

Please note: As a service to our authors and readers, this journal provides supporting information supplied by the authors. Such materials are peer-reviewed and may be re-organized for online delivery, but are not copy-edited or typeset by Wiley-Blackwell. Technical support issues arising from supporting information (other than missing files) should be addressed to the authors.

Acknowledgements

R.N.L. is supported by a Long-Term Fellowship from the International Human Frontier Science Program and a grant from the Kjell and Märta Beijers Foundation.

Abbreviations

AP, action potential; AVCN, anteroventral cochlear nucleus; EPSP, excitatory post-synaptic potential; HCN, hyperpolarization-activated cyclic-nucleotide gated; KO, knock-out; LSO, lateral superior olive; MAP2A/B, microtubule-associated protein 2A/B; MNTB, medial nucleus of the trapezoid body.

References

Adam, T.J., Finlayson, P.G. & Schwarz, D.W. (2001) Membrane properties of principal neurons of the lateral superior olive. *J. Neurophysiol.*, **86**, 922–934.

Bal, R. & Oertel, D. (2000) Hyperpolarization-activated, mixed-cation current (I(h)) in octopus cells of the mammalian cochlear nucleus. *J. Neurophysiol.*, **84**, 806–817.

Banks, M.I., Pearce, R.A. & Smith, P.H. (1993) Hyperpolarization-activated cation current (Ih) in neurons of the medial nucleus of the trapezoid body: voltage-clamp analysis and enhancement by norepinephrine and cAMP suggest a modulatory mechanism in the auditory brain stem. *J. Neurophysiol.*, **70**, 1420–1432.

Barnes-Davies, M., Barker, M.C., Osmani, F. & Forsythe, I.D. (2004) Kv1 currents mediate a gradient of principal neuron excitability across the tonotopic axis in the rat lateral superior olive. *Eur. J. Neurosci.*, **19**, 325–333.

Batra, R., Kuwada, S. & Fitzpatrick, D.C. (1997) Sensitivity to interaural temporal disparities of low- and high-frequency neurons in the superior olivary complex. I. Heterogeneity of responses. *J. Neurophysiol.*, **78**, 1222–1236.

Berger, T., Senn, W. & Luscher, H.R. (2003) Hyperpolarization-activated current Ih disconnects somatic and dendritic spike initiation zones in layer V pyramidal neurons. *J. Neurophysiol.*, **90**, 2428–2437.

Chevaleyre, V. & Castillo, P.E. (2002) Assessing the role of Ih channels in synaptic transmission and mossy fiber LTP. *Proc. Natl Acad. Sci. USA*, **99**, 9538–9543.

Desjardins, A.E., Li, Y.X., Reinker, S., Miura, R.M. & Neuman, R.S. (2003) The influences of Ih on temporal summation in hippocampal CA1 pyramidal neurons: a modeling study. *J. Comput. Neurosci.*, **15**, 131–142.

Kim, J.H., Sizov, I., Dobretsov, M. & von Gersdorff, H. (2007) Presynaptic Ca^{2}+ buffers control the strength of a fast post-tetanic hyperpolarization mediated by the alpha3 Na(+)/K(+)-ATPase. *Nat. Neurosci.*, **10**, 196–205.

Koch, U. & Grothe, B. (2003) Hyperpolarization-activated current (Ih) in the inferior colliculus: distribution and contribution to temporal processing. *J. Neurophysiol.*, **90**, 3679–3687.

Leao, R.N., Svahn, K., Berntson, A. & Walmsley, B. (2005) Hyperpolarization-activated (I) currents in auditory brainstem neurons of normal and congenitally deaf mice. *Eur. J. Neurosci.*, **22**, 147–157.

Leao, K.E., Leao, R.N., Sun, H., Fyffe, R.E. & Walmsley, B. (2006) Hyperpolarization-activated currents are differentially expressed in mice brainstem auditory nuclei. *J. Physiol.*, **576**, 849–864.

Leão, K.E., Leão, R.N., Deardorff, A.S., Garrett, A., Fyffe, R. & Walmsley, B. (2010) Sound stimulation modulates high-threshold K(+) currents in mouse auditory brainstem neurons. *Eur. J. Neurosci.*, **32**, 1658–1667.

Magee, J.C. (1999) Dendritic lh normalizes temporal summation in hippocampal CA1 neurons. *Nat. Neurosci.*, **2**, 508–514.

Marsalek, P. & Kofranek, J. (2005) Spike encoding mechanisms in the sound localization pathway. *Biosystems*, **79**, 191–198.

Migliore, M., Messineo, L. & Ferrante, M. (2004) Dendritic Ih selectively blocks temporal summation of unsynchronized sistal inputs in CA1 pyramidal neurons. *J. Comput. Neurosci.*, **16**, 5–13.

Nolan, M.F., Malleret, G., Dudman, J.T., Buhl, D.L., Santoro, B., Gibbs, E., Vronskaya, S., Buzsaki, G., Siegelbaum, S.A., Kandel, E.R. & Morozov, A. (2004) A behavioral role for dendritic integration: HCN1 channels constrain spatial memory and plasticity at inputs to distal dendrites of CA1 pyramidal neurons. *Cell*, **119**, 719–732.

Oviedo, H. & Reyes, A.D. (2005) Variation of input-output properties along the somatodendritic axis of pyramidal neurons. *J. Neurosci.*, **25**, 4985–4995.

Pape, H.C. (1996) Queer current and pacemaker: the hyperpolarization-activated cation current in neurons. *Annu. Rev. Physiol.*, **58**, 299–327.

Rothman, J.S. & Manis, P.B. (2003) The roles potassium currents play in regulating the electrical activity of ventral cochlear nucleus neurons. *J. Neurophysiol.*, **89**, 3097–3113.

Santoro, B. & Baram, T.Z. (2003) The multiple personalities of h-channels. *Trends Neurosci.*, **26**, 550–554.

Santoro, B., Liu, D.T., Yao, H., Bartsch, D., Kandel, E.R., Siegelbaum, S.A. & Tibbs, G.R. (1999) Identification of a gene encoding a hyperpolarization-activated pacemaker channel of brain. *Cell*, **93**, 717–729.

Schwartz, I.R. & Eager, P.R. (1999) Glutamate receptor subunits in neuronal populations of the gerbil lateral superior olive. *Hear. Res.*, **137**, 77–90.

Szalisznyo, K. (2006) Role of hyperpolarization-activated conductances in the lateral superior olive: a modeling study. *J. Comput. Neurosci.*, **20**, 137–152.

Tollin, D.J. & Yin, T.C. (2005) Interaural phase and level difference sensitivity in low-frequency neurons in the lateral superior olive. *J. Neurosci.*, **25**, 10648–10657.

Tsuchitani, C. (1988) The inhibition of cat lateral superior olive unit excitatory responses to binaural tone bursts. II. The sustained discharges. *J. Neurophysiol.*, **59**, 184–211.

Ulrich, D. & Stricker, C. (2000) Dendrosomatic voltage and charge transfer in rat neocortical pyramidal cells *in vitro*. *J. Neurophysiol.*, **84**, 1445–1452.

Willott, J.F. & Erway, L.C. (1998) Genetics of age-related hearing loss in mice. IV. Cochlear pathology and hearing loss in 25 BXD recombinant inbred mouse strains. *Hear. Res.*, **119**, 27–36.

Yamada, R., Kuba, H., Ishii, T.M. & Ohmori, H. (2005) Hyperpolarization-activated cyclic nucleotide-gated cation channels regulate auditory coincidence detection in nucleus laminaris of the chick. *J. Neurosci.*, **25**, 8867–8877.

Yin, T.C.T. (2002) Neural mechanisms of encoding binaural localization cues in the auditory brainstem. In: Fay, R.R., Oertle, D. & Popper, A.N. (Eds), *Integrative Functions in the Mammalian Auditory Pathway.* 1st ed. New York, USA: Springer, pp. 99–159.

Zacksenhouse, M., Johnson, D.H., Williams, J. & Tsuchitani, C. (1998) Single-neuron modeling of LSO unit responses. *J. Neurophysiol.*, **79**, 3098–3110.